AGU PUBLICATIONS

Geophysical Research Letters

RESEARCH LETTER
10.1002/2016GL068041

Key Points:
- Response time scales and regions of ocean heat uptake depend nonlinearly on the forcing level
- Global thermal expansion does not scale linearly with the surface temperature anomaly
- Reasons are forcing dependent circulation responses and the nonlinear equation of state

Supporting Information:
- Supporting Information S1

Correspondence to:
M. A. A. Rugenstein,
maria.rugenstein@env.ethz.ch

Citation:
Rugenstein, M. A. A., J. Sedláček, and R. Knutti (2016), Nonlinearities in patterns of long-term ocean warming, *Geophys. Res. Lett.*, *43*, doi:10.1002/2016GL068041.

Received 29 JAN 2016
Accepted 9 MAR 2016
Accepted article online 12 MAR 2016

Nonlinearities in patterns of long-term ocean warming

Maria A. A. Rugenstein[1], Jan Sedláček[1], and Reto Knutti[1]

[1]Institute for Atmospheric and Climate Science, ETH Zürich, Zürich, Switzerland

Abstract The ocean dominates the planetary heat budget and takes thousands of years to equilibrate to perturbed surface conditions, yet those long time scales are poorly understood. Here we analyze the ocean response over a range of forcing levels and time scales in a climate model of intermediate complexity and in the CMIP5 model suite. We show that on century to millennia time scales the response time scales, regions of anomalous ocean heat storage, and global thermal expansion depend nonlinearly on the forcing level and surface warming. As a consequence, it is problematic to deduce long-term from short-term heat uptake or scale the heat uptake patterns between scenarios. These results also question simple methods to estimate long-term sea level rise from surface temperatures, and the use of deep sea proxies to represent surface temperature changes in past climate.

1. Centennial Scale Ocean Heat Uptake in CMIP5 Models

Thermal expansion of ocean waters due to heat uptake from the atmosphere is a large contributor to recent and near-future sea level rise [*Church et al.*, 2011, 2013; *Levermann et al.*, 2013]. General circulation models (GCM) differ in the amplitude of simulated thermal expansion due to different base states, the total amount and vertical extent of the heat uptake, heat redistribution, and differences in the representation of vertical heat transport processes, advection, isopycnal, and diapycnal mixing [*Gregory*, 2000; *Kuhlbrodt and Gregory*, 2012; *Hallberg et al.*, 2012; *Church et al.*, 2013; *Exarchou et al.*, 2014; *Melet and Meyssignac*, 2015; *Liang et al.*, 2015]. Figures 1a–1c show zonal averaged ocean temperature anomaly patterns at the end of the century for three different scenarios simulated by the Coupled Model Intercomparison Project Phase 5 (CMIP5) models. Of the ocean heat uptake, 95–97% is confined to the upper kilometer, although locally, deep ocean heat uptake can contribute a large fraction of the total amplitude already decades after the perturbation [*Kuhlbrodt and Gregory*, 2012; *Marshall et al.*, 2014]. The standard deviation between the models increases with the forcing level and in Southern and Northern hemispheric high latitudes, but is generally smaller in magnitude than the mean signal shown in Figure 1, see also Figures S1–S3 in the supporting information, [*Yin*, 2012; *Sallée et al.*, 2013; *Heuzé et al.*, 2015]. Figures 1d – 1f demonstrate that locally, pattern scaling between the different scenarios is not possible with high accuracy [*Bilbao et al.*, 2015]. If the ocean warming pattern would respond linearly to the surface forcing the differences between the scaled scenarios in the upper row should be zero. However, the lower forced scenario takes up relatively more heat into the Southern Ocean and to low latitude intermediate depth of around 500–2000 m (Figure 1d) than the intermediate and higher forced scenarios (Figure 1f). In the surface ocean higher forcing leads to relatively more heat uptake (see also Figure S1 in the supporting information for a zoom into the upper ocean).

The near-future sea level rise has been studied extensively but is also known to be a poor indicator of centennial, millennial, or equilibrated conditions [e.g., *Stouffer and Manabe*, 2003; *Li et al.*, 2013], but only very few GCMs have been run over millennia due to computational cost. Here we explore the centennial to millennia patterns of ocean warming and their dependence on time and on forcing levels. We show that long-term thermal expansion is not proportional to surface warming. Deduction of one time frame frame or forcing scenario to another is limited, not only for the transient response as shown for the CMIP5 models but also for equilibrated conditions.

2. Model and Simulations

To explore the limits of scaling over a wide range of forcing levels and time scales up to equilibrium, we use the intermediate complexity model (EMIC) ECBILT-CLIO, which consists out of an ocean, sea ice, and atmospheric component. The ocean general circulation model has a free surface, 20 unevenly spaced layers,

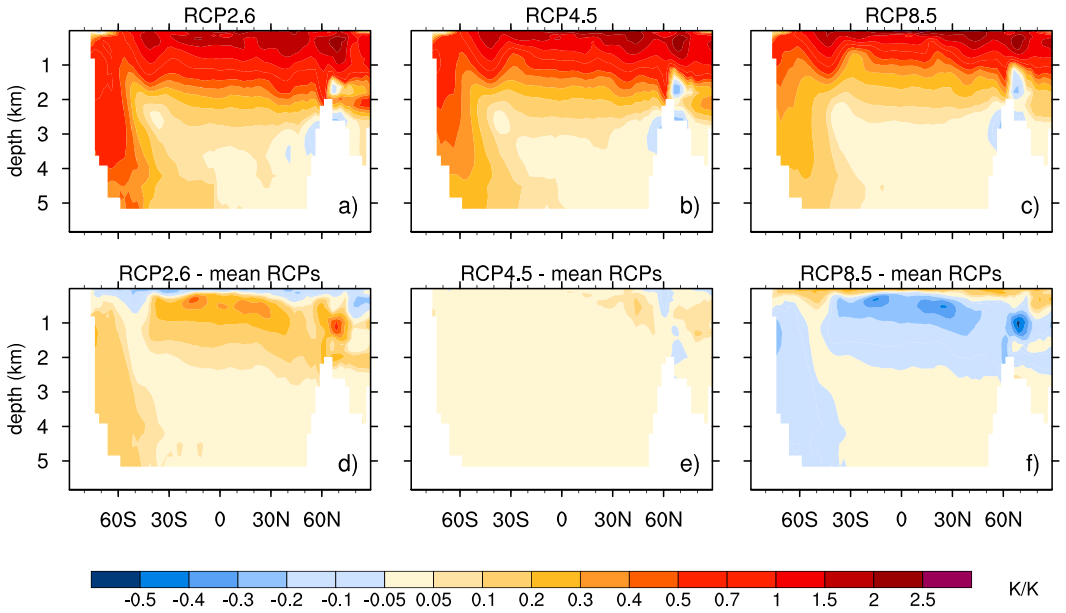

Figure 1. Zonal mean ocean temperature anomaly averaged over year 2081 to 2100 and normalized with the average ocean temperature of (a) Representative Concentration Pathways (RCP) 2.6, (b) RCP4.5, and (c) RCP8.5 of 14 CMIP5 models, described in *Collins et al.* [2013, Figure 12.12]. Differences between (d) RCP2.6, (e) RCP4.5, (f) RCP8.5, and the mean of the three RCPs. The color scale is not linear (around 0 and above 0.5). See Figures S1–S3 in the supporting information for more details on each model.

a 3° × 3° horizontal resolution, and a thermodynamic-dynamic sea ice model (*Goosse and Fichefet* [1999], and more details on the model formulation in the supporting information). The atmospheric model solves the quasi-geostrophic equations on a spectral grid with three vertical levels and a horizontal resolution of 5.6° × 5.6°, parameterizations of diabatic heating and surface heat fluxes, and prescribed seasonal varying cloud cover [*Opsteegh et al.*, 2011]. This results in a low Equilibrium Climate Sensitivity (ECS) of 1.7 K (see also *Friedrich et al.* [2010], *Levermann et al.* [2013], *Eby et al.* [2013], and *Church et al.* [2013], and references therein). Given the limitations of the model, we emphasize that we aim at insight and not prediction. We will interpret the scenarios relative to each other, rather than their absolute values compared to other models with the same forcing. The advantage of the model is that large ensembles of hundreds of members and simulations of 10,000 years are possible, a range unfeasible with a full general circulation model.

We conduct a range of step forcing experiments, each consisting—roughly according to the ratio of anomaly signal to internal variability noise—of several initial condition ensemble members: 1.07 times preindustrial CO_2 concentrations of 280 ppm (90 members), 1.4xCO_2 (90 members), 2xCO_2 (50 members), 4xCO_2 (20 members), 8xCO_2 (20 members), and 16xCO_2 (10 members), each 1000 years long. The forcing levels are chosen to simulate roughly no change in circulation for the very low forced cases to an initially strongly stratified response and large heat uptake for the high forced cases. One member of each forcing level is further integrated to 10,000 years. We show anomalies of these simulations with 1000 or 10,000 year long control simulations (no CO_2 change, 94 initial condition ensemble members). Thus, each ensemble member's anomaly is determined with a slightly different control simulation. The temperature of the control simulations shows no drift, but the salinity shows both a small linear control run drift (globally 0.05 kg m^{-3} per 10,000 yrs) and a smaller forcing level dependent drift, due to the handling of the sea ice. Both drifts are accounted for by scaling the salinity pattern at each time step, location, and forcing level with the drift, so that the global mean salinity is constant at all times, but allowed to change its spatial pattern.

3. Equilibration of Ocean Heat Uptake and Circulation Changes

Figures 2a–2d show—analogous to Figure 1—the equilibrium zonally averaged ocean temperature anomalies normalized with the equilibrium global ocean temperature for four representative scenarios in color, and the unscaled changes in salinity in grey contours. The temperature anomaly is not distributed homogeneously even though the global ocean temperature is in equilibrium with the surface. This agrees with

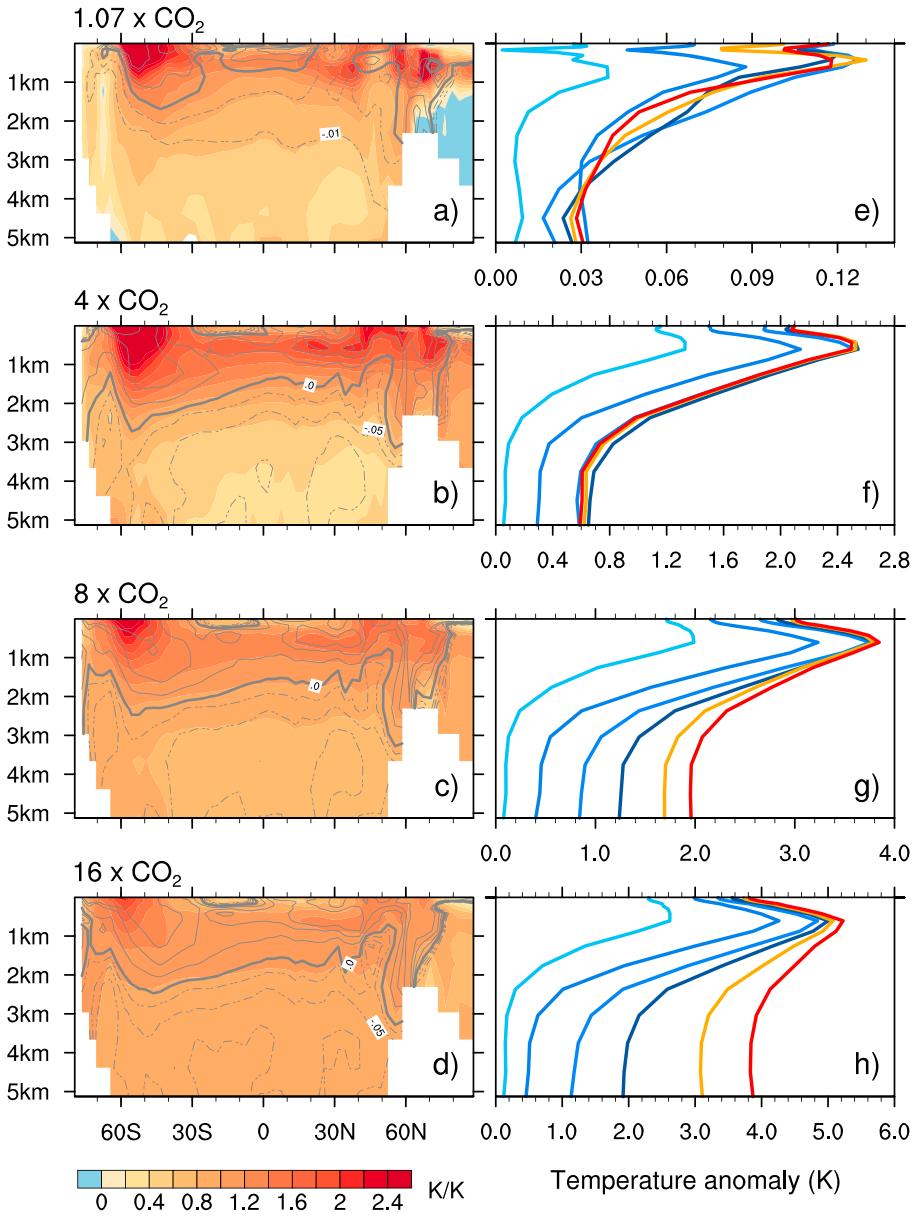

Figure 2. (a–d) Zonal average equilibrium (years 9000–10,000) ocean warming pattern for four forcing scenarios, normalized with the average ocean temperature of that time frame. Gray lines show salinity anomaly contours of −0.075, −0.05, −0.025 (dashed), 0 (thick), and 0.05, 0.1, 0.15 psu (dashed) unscaled. (e–h) Time evolution of global average warming at all depths for the same scenarios. Lines from light blue to dark blue to red indicate 100 year averages around year 100, 300, 600, 1000, 2000, and 9900 after the perturbation. Only the single long simulations are used for this figure. Scale for Figures 2e–2h changes.

models showing gradients of several degrees [*Gillett et al.*, 2011 and *Knutti*, 2002] but disagrees with the rather homogeneous warming patterns of *Stouffer and Manabe* [2003] and *Li et al.* [2013], in which the vertical gradient of temperature is less than 1.5 K. Contrary to the transient pattern analyses of *Kuhlbrodt and Gregory* [2012] and *Melet and Meyssignac* [2015], the equilibrated simulations do not scale with their global temperature especially in the Southern Ocean, which is widely recognized to be important in shaping the transient and equilibrium global heat uptake [e.g., *Schneider and Thompson*, 1981; *Manabe and Stouffer*, 1994; *Bi et al.*, 2001; *Bryan et al.*, 2006]. The Northern Hemisphere high latitudes become relatively more important in lower forced scenarios, as suggested also in Figures 1d–1f. Salinity and temperature anomalies roughly follow the same pattern but impact the density in opposite ways through the equation of state. In regions with increased warming, the salinity anomaly is positive, thus compensating the change in density due to the increased heat

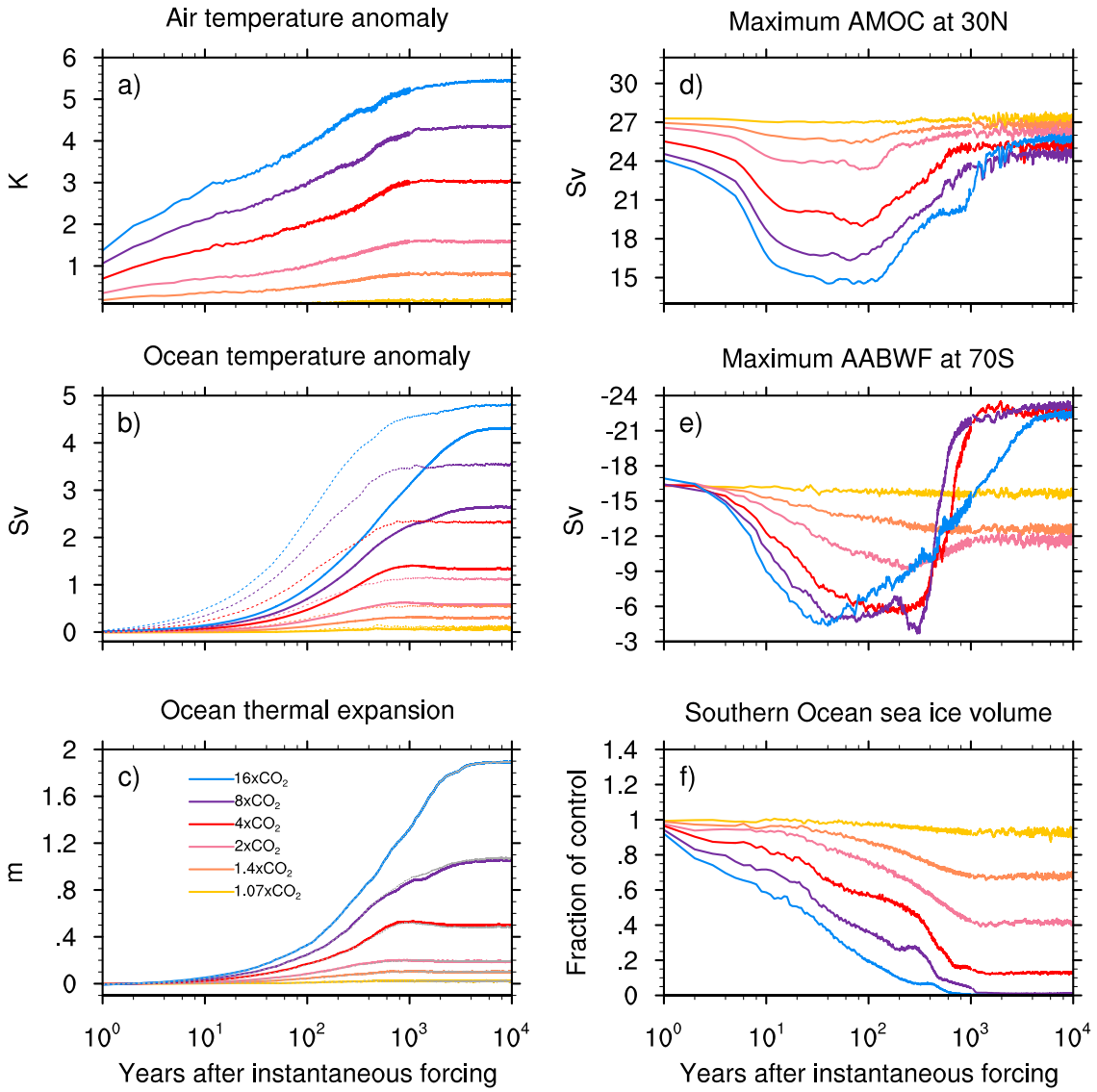

Figure 3. Time evolution of (a) global average surface air temperature anomaly, (b) global average ocean temperature anomaly for the whole (solid) and uppermost kilometer ocean (dashed), (c) global average ocean thermal expansion, gray lines are explained in the text. (d) maximum Atlantic Meridional Overturning Circulation at 30°N, (e) Antarctic Bottom Water Formation, as maximum of overturning at 70°S, and (f) the sea ice volume, expressed as fraction of the control simulation value. In all panels, years 1–1000 are the annual and ensemble average; years 1000–10,000 are a 100 year running mean of one simulation for each forcing level.

content [*Lowe and Gregory*, 2006]. This explains why the maximum warming can be sustained in the tropical subsurface ocean without destabilizing the water column [*Yin et al.*, 2011]. Figures 2e–2h show the time evolution of global ocean warming with depth. While the higher forced scenarios take longer to equilibrate, they are more efficient in transporting the anomaly into the deep ocean. However, in taking the average subsurface maximum versus deep ocean temperature as an indicator of homogeneity, we find that the vertical gradient does not evolve linearly with the forcing level: The subsurface maximum warming is a factor of 3.3, 5, 7, 4.3, 1.9, and 1.2 greater than the deep ocean warming for the scenarios of 1.07, 1.4, 2, 4, 8, and 16xCO_2. On century time scales, for very low forced scenarios, even negative deep ocean temperature trends are possible (Figure 2e, blue lines). This is consistent with slightly decreasing trends in recent decadal observations [*Wunsch and Heimbach*, 2014; *Llovel et al.*, 2014; *Liang et al.*, 2015]. Locally, slightly negative and positive trends can occur after the upper 2000 m are fully equilibrated.

Figure 3 further explains the time evolution of the different forcing scenarios. All panels share the same color coding (ranging from 1.07 in yellow to 16xCO_2 in blue) and logarithmic time axis. The global average surface

air temperature anomaly (Figure 3a) scales only roughly with the forcing level (i.e., the equilibrium climate sensitivity for higher forcings is less than expected from linearly scaling up lower forcing levels). Figure 3b shows the global average ocean temperature anomaly with the global value as solid and the uppermost kilometer evolution as dashed lines. In some scenarios, the deep ocean reaches its equilibrium value at almost the same time scale as the upper ocean ($4xCO_2$), while for other scenarios it takes several thousand years longer ($8xCO_2$), dependent on stratification, overturning, and mixing response. Figure 3c depicts the sea level rise due to ocean thermal expansion and salinity changes, calculated from the global detrended in situ density anomaly, volume, control run reference density, and surface area. The gray dashed lines show the sea level rise due to thermal expansion only, assuming a constant salinity pattern. While locally, the salinity changes are important to set the dynamics and sea level change, globally, they are negligible. In equilibrium, the deep ocean (below 1 km) accounts for 64, 55, 60, 67, and 72% of the total thermal expansion for the 1.07, 1.4, 2, 4, and $16xCO_2$ forcing, respectively. This compares well with the 60% contribution of the deep (below 1.5 km) ocean of the general circulation model of *Li et al.* [2013].

The patterns of ocean heat uptake and redistribution, as well as changes in the patterns of salinity depend on circulation changes, thus on surface temperature anomaly and the forcing level. The Atlantic Meridional Overturning Circulation (AMOC, Figure 3d), here defined as the maximum in the stream function at 30°N, initially declines, as expected, more with a higher forcing level [*Manabe and Stouffer*, 1994; *Gregory et al.*, 2005; *Zhu et al.*, 2014]. However, both the recovery level and recovery rate vary with the forcing level and some scenarios recover to a greater degree than others. While almost all GCMs and EMICs show a reduction of the AMOC with increased radiative forcing, the time and strength of the recovery differs strongly between them [*Stouffer and Manabe*, 2003; *Li et al.*, 2013; *Zickfeld et al.*, 2013]. The recovery or increased instability can be caused by a surface salt advection feedback [*Latif et al.*, 2000; *Bryan et al.*, 2013] or increased bottom water temperatures due to slower Antarctic Bottom Water Formation (AABWF) [*Manabe and Stouffer*, 1994; *Stouffer and Manabe*, 2003]. Since the stronger the AMOC declines, the more heat can be taken up by the deep North Atlantic [*Rugenstein et al.*, 2013], the very strong reduction and slow recovery in the higher forced cases likely causes the more vertically homogeneous equilibrium temperature anomaly (Figure 2).

Finally, Figures 3e and 3f show the time evolution the AABWF strength—defined as maximum overturning at 70°S—and the sea ice volume—depicted as fraction of the control run value. The AABWF reduces in all cases, but does not scale linearly with the radiative forcing. The time of minimum AABWF, the recovery or overshooting amplitude, and rate of recovery vary several thousand years between the different forcing cases. The reason for the recovery is not well understood and attributable to either the long-term warming or the salinization of the deep ocean, destabilizing the water column from below [*Manabe and Stouffer*, 1994; *Bi et al.*, 2001], or strong enough convective events triggered by changed seasonality [*Yamamoto et al.*, 2015]. The higher forced levels, which show relatively more deep ocean warming (Figure 2), indeed recover and overshoot. The Southern Ocean sea ice reduces in all cases roughly proportional to the forcing level until year 20, before the rate of change as well as the equilibrium level becomes forcing level dependent.

4. Thermal Expansion

We now explore the consequences of the inhomogeneous and forcing dependent warming pattern on the sea level rise due to thermal expansion. Previous studies used the equilibrium surface temperature anomaly as dependent variable and found an approximately linear relation to the thermal expansion [*Knutti and Stocker*, 2000; *Meehl et al.*, 2007; *Levermann et al.*, 2013], but the evidence for this is mostly based on intermediate complexity, 2.5-D or single basin models. However, there is no physical reason why this should be the case, and *Pardaens et al.* [2011] and *Körper et al.* [2013] find indeed, but do not explain, nonlinearities for transient states at the end of the century for several GCMs. We discuss three mechanisms which impact the relationship between the thermal expansion and surface temperature anomaly (Figure 4).

1. The nonlinearity of the equation of state: The expansion coefficient of sea water increases with warmer temperature and lower pressure [e.g., *Palter et al.*, 2014].
2. The transient effects of taking up more heat with time but moving a larger fraction of heat into the deep ocean, where thermal expansion is less.
3. The forcing level and circulation-dependent heat uptake as discussed in Figures 2 and 3.

Knutti and Stocker [2000] pointed out that thermal expansion is 0.5 m higher with a shutdown AMOC compared to a state of the same forcing and recovered AMOC or North Pacific overturning. We reproduce this

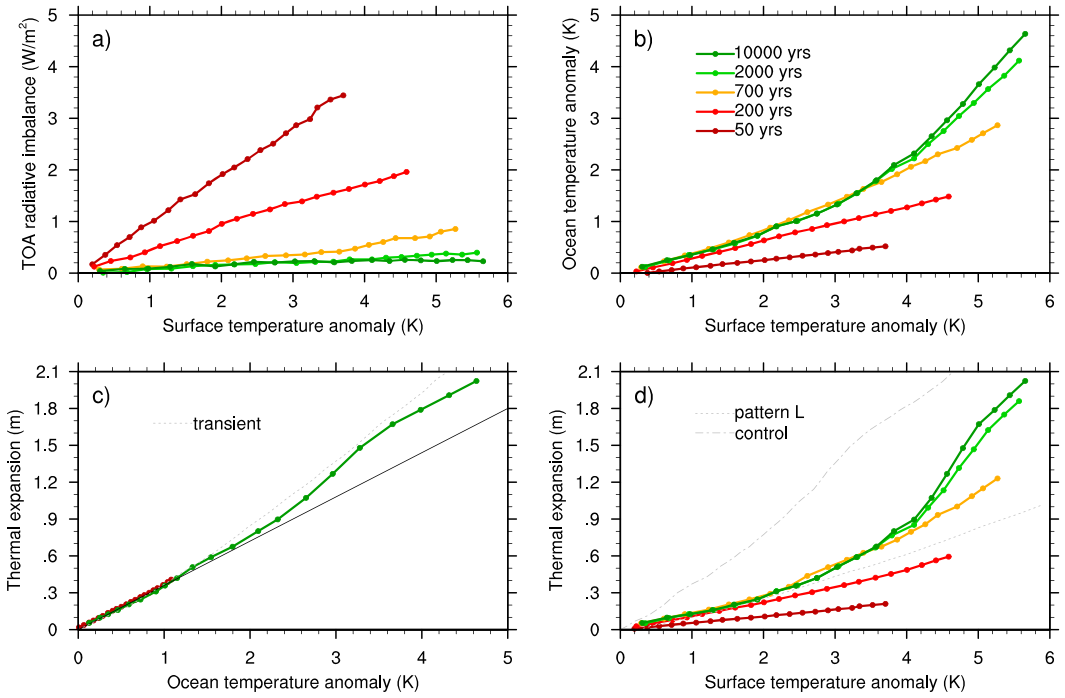

Figure 4. (a) Top of the Atmosphere (TOA) radiative imbalance versus global surface temperature anomaly averages around year 50, 200, 700, 2000, and 10 000. (b) Global ocean temperatures versus global surface temperature anomalies, (c) Global sea level rise due to thermal expansion versus global ocean temperature anomaly. Constructed thermal expansion without circulation change and a linear (black) or nonlinear (gray) equation of state. (d) Thermal expansion versus global surface temperature anomaly (color) and constructed thermal expansion based on a pattern of equilibrated warming at $1.07xCO_2$ (pattern L) and a uniform anomaly added to the control simulation pattern (control, both dashed gray).

result in ECBILT-CLIO through a fresh water perturbation in the North Atlantic and the sea level rise due to the AMOC collapse—without any radiative forcing—is 0.3 m.

To fill up gaps between simulations shown above and to explore higher warming levels, we show 18 additional simulations (depicted by dots in Figure 4). The lowest forcing is $1.15xCO_2$ (dots farthest left), increasing in steps of $2^{0.2}$ up to $2^{4.4} = 21xCO_2$ (dots on the far right). The surface temperature sensitivity even becomes lower at high CO_2 values, so $21xCO_2$ should not be interpreted at face value. The time dimension is depicted in colors, showing five decadal to millennia time slices. Figures 4a and 4b show that the total ocean heat uptake (which dominates the Top of the Atmosphere (TOA) radiative imbalance), is linearly related to the surface air temperature anomaly at all times, but does not translate into a linear relationship between the ocean and surface air temperature anomalies on centennial to millennial time scales. For one unit of surface warming the ocean warms more through time (equilibration, curves moving up) and higher forcing levels (circulation changes, curves bend up, see also Figures 2 and 3). Figure 4c brings the equation of state into play: The sea level rise due to thermal expansion is linearly related to the ocean temperature anomaly on decadal time scales (dark red line). If the equation of state were linear and the circulation was constant, the equilibrium values would lie on the black line, far away from the equilibrated model output (green line). To assess how much of this nonlinearity is due to the equation of state, we use the 3-D warming and salinity pattern after 50 years and linearly scale it up, mimicking 5K warming under the assumption of no circulation change. We then calculate the thermal expansion with the nonlinear equation of state (*McDougall et al.* [2003], rho_mwif function, see also supporting information, gray dashed line). The green line is close to that estimate; i.e., the greatest part of the nonlinearity of the equilibrated situation is due to the fact that the equation of state is nonlinear. The remaining discrepancy between the gray and green line is due to the effect that for longer time scales and higher forcing levels more heat is transported from the surface layers to the deep ocean. Figure 4d brings all effects together, showing that thermal expansion from centennial time scales onward—increasingly with higher forcing levels—is nonlinearly related to the surface temperature anomaly. The dashed gray lines show again two artificially constructed cases to assess the impact of the nonlinear equation of state without

circulation changes (explained in the supporting information). In summary, thermal expansion is approximately proportional to the atmospheric warming on time scales of a century and for small forcings, but on long time scales or for stronger forcings the linearity assumption is no longer valid. The reasons are that the globally integrated heat uptake itself is not proportional to surface warming and that the distribution of warming changes with changes in circulation and mixing, which in combination with the nonlinearity of the equation of states affects thermal expansion.

5. Implications for Paleo and Modern Studies

A common assumption in paleo-oceanography is that the temperature (anomaly) of the intermediate or deep ocean — indicated by, e.g., benthic foraminifera — represents a time averaged (sea) surface temperature (SST) record of the regions where deep waters formed [e.g., *Savin*, 1977; *Huber*, 1998; *Zachos et al.*, 2001; *Voigt et al.*, 2004; *Cramer et al.*, 2009; *Friedrich et al.*, 2012] or the SST anomalies represent deep ocean temperature anomalies [*Jaccard et al.*, 2014]. Modeling studies found that the deep water temperature anomaly was the same as the southern high latitude SST anomaly [*Manabe and Bryan*, 1985] or that it resembles the SST anomaly of low latitude [*Stouffer and Manabe*, 2003]. We find that the anomalous heat uptake by the intermediate and deep ocean does not correspond to the atmospheric temperature increase at low or high latitudes. This implies that, without knowledge of forcing and circulation history, the interpretation of ocean temperature proxies beyond their region may be more problematic than currently appreciated. Another long-term implication of our finding concerns climate sensitivity. Figure 3a indicates that the effective climate sensitivity in the model increases with increased temperatures for all simulations (see more elaborate argument in *Knutti and Rugenstein* [2015]). This implies that potentially, ocean circulation can have a large effect on the TOA radiative imbalance even in the absence of a cloud feedback. A more general consequence concerns the marine carbon climate feedback and regions of melting sea ice, which both are likely influenced by the places of anomalous heat storage and thus, dependent on the forcing history [*Randerson et al.*, 2015]. Finally, and also on shorter time scales, pattern scaling between scenarios might break down already at the end of this century or more likely in future centuries. We therefore cannot infer future or past equilibria from transient behavior or past transient behavior from equilibria. A detailed knowledge of the dependence of circulation responses to different forcing levels and scenarios is key to understand and compare not only transient but also equilibrium warming patterns.

In summary, although for subcentennial time scales and low forcing levels the linear relationship between thermal expansion and surface temperature anomaly seems to hold, our analysis suggests that we do not properly understand the centennial to millennia ocean warming patterns, mainly due to a limited understanding of circulation and mixing changes. Complex enough models — simulating long enough time scales and different ranges of scenarios (as, e.g., in *Krasting et al.* [2016]) — are necessary to explore these effects.

Acknowledgments
We thank Thomas Frölicher, Axel Timmermann, Summer Praetorius, and two anonymous reviewers for comments and discussions. We acknowledge the World Climate Research Programme's Working Group on Coupled Modelling, which is responsible for CMIP, and we thank the climate modeling groups (listed in Figure S3 of the supporting information) for producing and making available their model output. For CMIP the U.S. Department of Energy's Program for Climate Model Diagnosis and Intercomparison provides coordinating support and led development of software infrastructure in partnership with the Global Organization for Earth System Science Portals. Data from the EMIC used here are available upon request from the authors. ECBILT–CLIO is free to download from KNMI at http://www.sciamachy-validation.org/research/CKO/ecbilt.html.

References

Bi, D., W. F. Budd, A. C. Hirst, and X. Wu (2001), Collapse and reorganisation of the Southern Ocean overturning under global warming in a coupled model, *Geophys. Res. Lett.*, *28*(20), 3927–3930, doi:10.1029/2001GL013705.

Bilbao, R. A., J. M. Gregory, and N. Bouttes (2015), Analysis of the regional pattern of sea level change due to ocean dynamics and density change for 1993–2099 in observations and CMIP5 AOGCMs, *Clim. Dyn.*, *45*(9–10), 2647–2666, doi:10.1007/s00382-015-2499-z.

Bryan, F., N. Nakashiki, Y. Yoshida, and K. Maruyama (2013), Response of the meridional overturning circulation during differing pathways toward greenhouse gas stabilization, in *Ocean Circulation: Mechanisms and Impacts — Past and Future Changes of Meridional Overturning*, edited by F. Bryan et al., pp. 351–363, AGU, Washington, D. C., doi:10.1029/173GM22.

Bryan, F. O., G. Danabasoglu, N. Nakashiki, Y. Yoshida, D.-H. Kim, J. Tsutsui, and S. C. Doney (2006), Response of the North Atlantic thermohaline circulation and ventilation to increasing carbon dioxide in CCSM3, *J. Clim.*, *19*(11), 2382–2397, doi:10.1175/JCLI3757.1.

Church, J. A., N. J. White, L. F. Konikow, C. M. Domingues, J. G. Cogley, E. Rignot, J. M. Gregory, M. R. van den Broeke, A. J. Monaghan, and I. Velicogna (2011), Revisiting the Earth's sea-level and energy budgets from 1961 to 2008, *Geophys. Res. Lett.*, *38*, L18601, doi:10.1029/2011GL048794.

Church, J. A., et al. (2013), Sea level change, in *Climate Change 2013: The Physical Science Basis. Contribution of Working Group I to the Fifth Assessment Report of the Intergovernmental Panel on Climate Change*, edited by T. Stocker et al., Cambridge Univ. Press, Cambridge, U. K., and New York.

Collins, M., et al. (2013), Long-term climate change: Projections, commitments and irreversibility, in *Climate Change 2013: The Physical Science Basis. Contribution of Working Group I to the Fifth Assessment Report of the Intergovernmental Panel on Climate Change*, edited by T. Stocker et al., Cambridge Univ. Press, Cambridge, U. K., and New York.

Cramer, B. S., J. R. Toggweiler, J. D. Wright, M. E. Katz, and K. G. Miller (2009), Ocean overturning since the Late Cretaceous: Inferences from a new benthic foraminiferal isotope compilation, *Paleoceanography*, *24*, PA4216, doi:10.1029/2008PA001683.

Eby, M., et al. (2013), Historical and idealized climate model experiments: An intercomparison of Earth system models of intermediate complexity, *Clim. Past*, *9*(3), 1111–1140, doi:10.5194/cp-9-1111-2013.

Exarchou, E., T. Kuhlbrodt, J. M. Gregory, and R. S. Smith (2014), Ocean heat uptake processes: A model intercomparison, *J. Clim.*, *28*(2), 887–908, doi:10.1175/JCLI-D-14-00235.1.

Friedrich, O., R. D. Norris, and J. Erbacher (2012), Evolution of middle to Late Cretaceous oceans—A 55 m.y. record of Earth's temperature and carbon cycle, *Geology*, *40*(2), 107–110, doi:10.1130/g32701.1.

Friedrich, T., A. Timmermann, L. Menviel, O. Elison Timm, A. Mouchet, and D. M. Roche (2010), The mechanism behind internally generated centennial-to-millennial scale climate variability in an Earth system model of intermediate complexity, *Geosci. Model Dev.*, *3*(2), 377–389, doi:10.5194/gmd-3-377-2010.

Gillett, N. P., V. K. Arora, K. Zickfeld, S. J. Marshall, and W. J. Merryfield (2011), Ongoing climate change following a complete cessation of carbon dioxide emissions, *Nat. Geosci.*, *4*(2), 83–87.

Goosse, H., and T. Fichefet (1999), Importance of ice-ocean interactions for the global ocean circulation: A model study, *J. Geophys. Res.*, *104*(C10), 23,337–23,355, doi:10.1029/1999JC900215.

Gregory, J. M. (2000), Vertical heat transports in the ocean and their effect on time-dependent climate change, *Clim. Dyn.*, *16*, 501–515, doi:10.1007/s003820000059.

Gregory, J. M., et al. (2005), A model intercomparison of changes in the Atlantic thermohaline circulation in response to increasing atmospheric CO_2 concentration, *Geophys. Res. Lett.*, *32*, L12703, doi:10.1029/2005GL023209.

Hallberg, R., A. Adcroft, J. P. Dunne, J. P. Krasting, and R. J. Stouffer (2012), Sensitivity of twenty-first-century global-mean steric sea level rise to ocean model formulation, *J. Cli.*, *26*(9), 2947–2956, doi:10.1175/JCLI-D-12-00506.1.

Heuzé, C., K. J. Heywood, D. P. Stevens, and J. K. Ridley (2015), Changes in global ocean bottom properties and volume transports in CMIP5 models under climate change scenarios, *J. Clim.*, *28*(8), 2917–2944, doi:10.1175/JCLI-D-14-00381.1.

Huber, B. T. (1998), Tropical paradise at the cretaceous poles?, *Science*, *282*(5397), 2199–2200, doi:10.1126/science.282.5397.2199.

Jaccard, S., E. D. Galbraith, T. L. Frölicher, and N. Gruber (2014), Ocean (de)oxygenation across the last deglaciation: Insights for the future, *Oceanography*, *27*(1), 26–35.

Knutti, R. (2002), Modelling studies on the probability and predictability of future climate change, PhD thesis, p. 138, Phys. Inst., Univ. of Bern, Bern, Switzerland.

Knutti, R., and M. A. A. Rugenstein (2015), Feedbacks, climate sensitivity and the limits of linear models, *Philos. Trans. R. Soc. A*, *373*(2054), 20150146, doi:10.1098/rsta.2015.0146.

Knutti, R., and T. F. Stocker (2000), Influence of the thermohaline circulation on projected sea level rise, *J. Clim.*, *13*(12), 1997–2001, doi:10.1175/1520-0442(2000)0131997:IOTTCO2.0.CO;2.

Körper, J., et al. (2013), The effects of aggressive mitigation on steric sea level rise and sea ice changes, *Clim. Dyn.*, *40*(3–4), 531–550, doi:10.1007/s00382-012-1612-9.

Kuhlbrodt, T., and J. Gregory (2012), Ocean heat uptake and its consequences for the magnitude of sea level rise and climate change, *Geophys. Res. Lett.*, *39*, L18608, doi:10.1029/2012GL052952.

Krasting, J. P., J. P. Dunne, R. J. Stouffer, and R. W. Hallberg (2016), Enhanced Atlantic sea-level rise relative to the Pacific under high carbon emission rates, *Nat. Geosci.*, *9*, 210–214, doi:10.1038/ngeo2641.

Latif, M., E. Roeckner, U. Mikolajewicz, and R. Voss (2000), Tropical stabilization of the thermohaline circulation in a greenhouse warming simulation, *J. Clim.*, *13*(11), 1809–1813, doi:10.1175/1520-0442(2000)0131809:L2.0.CO;2.

Levermann, A., P. U. Clark, B. Marzeion, G. A. Milne, D. Pollard, V. Radic, and A. Robinson (2013), The multimillennial sea-level commitment of global warming, *Proc. Natl. Acad. Sci. U.S.A.*, *110*(34), 13,745–13,750, doi:10.1073/pnas.1219414110.

Li, C., J.-S. Storch, and J. Marotzke (2013), Deep-ocean heat uptake and equilibrium climate response, *Clim. Dyn.*, *40*(50–6), 1071–1086, doi:10.1007/s00382-012-1350-z.

Liang, X., C. Wunsch, P. Heimbach, and G. Forget (2015), Vertical redistribution of oceanic heat content, *J. Clim.*, *28*(9), 3821–3833, doi:10.1175/JCLI-D-14-00550.1.

Llovel, W., J. K. Willis, F. W. Landerer, and I. Fukumori (2014), Deep-ocean contribution to sea level and energy budget not detectable over the past decade, *Nature Clim. Change*, *4*, 1031–1035, doi:10.1038/nclimate2387.

Lowe, J. A., and J. M. Gregory (2006), Understanding projections of sea level rise in a Hadley Centre coupled climate model, *J. Geophys. Res.*, *111*, C11014, doi:10.1029/2005JC003421.

Manabe, S., and K. Bryan (1985), CO_2-induced change in a coupled ocean-atmosphere model and its paleoclimatic implications, *J. Geophys. Res.*, *90*(C6), 11,689–11,707, doi:10.1029/JC090iC06p11689.

Manabe, S., and R. J. Stouffer (1994), Multiple-century response of a coupled ocean-atmosphere model to an increase of atmospheric carbon dioxide, *J. Clim.*, *7*(1), 5–23, doi:10.1175/1520-0442(1994)0070005:MCROAC2.0.CO;2.

Marshall, J., J. R. Scott, K. C. Armour, J.-M. Campin, M. Kelley, and A. Romanou (2014), The ocean's role in the transient response of climate to abrupt greenhouse gas forcing, *Clim. Dyn.*, *44*(7), 2287–2299, doi:10.1007/s00382-014-2308-0.

McDougall, T. J., D. R. Jackett, D. G. Wright, and R. Feistel (2003), Accurate and computationally efficient algorithms for potential temperature and density of seawater, *J. Atmos. Oceanic Technol.*, *20*(5), 730–741, doi:10.1175/1520-0426(2003)20730:AACEAF2.0.CO;2.

Meehl, G. A., et al. (2007), Global climate projections, in *Climate Change 2007: The Physical Science Basis. Contribution of Working Group I to the Fourth Assessment Report of the Intergovernmental Panel on Climate Change*, edited by S. Solomon et al., Cambridge Univ. Press, Cambridge, U. K., and New York.

Melet, A., and B. Meyssignac (2015), Explaining the spread in global mean thermosteric sea level rise in CMIP5 climate models, *J. Clim.*, *28*, 9918–9940, doi:10.1175/JCLI-D-15-0200.1.

Opsteegh, J., R. Haarsma, F. Selten, and A. Kattenberg (2011), ECBILT: A dynamic alternative to mixed boundary conditions in ocean models, *Tellus A*, *50*(3), 348–367.

Palter, J. B., S. M. Griffies, B. L. Samuels, E. D. Galbraith, A. Gnanadesikan, and A. Klocker (2014), The deep ocean buoyancy budget and its temporal variability, *J. Clim.*, *27*(2), 551–573, doi:10.1175/JCLI-D-13-00016.1.

Pardaens, A. K., J. A. Lowe, S. Brown, R. J. Nicholls, and D. de Gusmão (2011), Sea-level rise and impacts projections under a future scenario with large greenhouse gas emission reductions, *Geophys. Res. Lett.*, *38*, L12604, doi:10.1029/2011GL047678.

Randerson, J. T., K. Lindsay, E. Munoz, W. Fu, J. K. Moore, F. M. Hoffman, N. M. Mahowald, and S. C. Doney (2015), Multicentury changes in ocean and land contributions to the climate-carbon feedback, *Global Biogeochem. Cycles*, *29*, 744–759, doi:10.1002/2014GB005079.

Rugenstein, M. A. A., M. Winton, R. J. Stouffer, S. M. Griffies, and R. Hallberg (2013), Northern high-latitude heat budget decomposition and transient warming, *J. Clim.*, *26*(2), 609–621, doi:10.1175/JCLI-D-11-00695.1.

Sallée, J. B., E. Shuckburgh, N. Bruneau, A. J. S. Meijers, T. J. Bracegirdle, Z. Wang, and T. Roy (2013), Assessment of Southern Ocean water mass circulation and characteristics in CMIP5 models: Historical bias and forcing response, *J. Geophys. Res. Oceans*, *118*, 1830–1844, doi:10.1002/jgrc.20135.

Savin, S. M. (1977), The history of the Earth's surface temperature during the past 100 million years, *Annu. Rev. Earth. Planet. Sci.*, *5*(1), 319–355, doi:10.1146/annurev.ea.05.050177.001535.

Schneider, S. H., and S. L. Thompson (1981), Atmospheric CO_2 and climate: Importance of the transient response, *J. Geophysical Res.*, *86*(C4), 3135–3147, doi:10.1029/JC086iC04p03135.

Stouffer, R., and S. Manabe (2003), Equilibrium response of thermohaline circulation to large changes in atmospheric CO_2 concentration, *Clim. Dyn.*, *20*(7–8), 759–773, doi:10.1007/s00382-002-0302-4.

Voigt, S., A. S. Gale, and S. Flögel (2004), Midlatitude shelf seas in the Cenomanian-Turonian greenhouse world: Temperature evolution and North Atlantic circulation, *Paleoceanography*, *19*, PA4020, doi:10.1029/2004PA001015.

Wunsch, C., and P. Heimbach (2014), Bidecadal thermal changes in the abyssal ocean, *J. Phys. Oceanogr.*, *44*(8), 2013–2030, doi:10.1175/JPO-D-13-096.1.

Yamamoto, A., A. Abe-Ouchi, M. Shigemitsu, A. Oka, K. Takahashi, R. Ohgaito, and Y. Yamanaka (2015), Global deep ocean oxygenation by enhanced ventilation in the Southern Ocean under long-term global warming, *Global Biogeochem. Cycles*, *29*, 1801–1815, doi:10.1002/2015GB005181.

Yin, J. (2012), Century to multi-century sea level rise projections from CMIP5 models, *Geophys. Res. Lett.*, *39*, L17709, doi:10.1029/2012GL052947.

Yin, J., J. T. Overpeck, S. M. Griffies, A. Hu, J. L. Russell, and R. J. Stouffer (2011), Different magnitudes of projected subsurface ocean warming around Greenland and Antarctica, *Nat. Geosci.*, *4*(8), 524–528.

Zachos, J. C., M. Pagani, L. C. Sloan, E. Thomas, and K. Billups (2001), Trends, rhythms, and aberrations in global climate 65 Ma to present, *Science*, *292*(5517), 686–693, doi:10.1126/science.1059412.

Zhu, J., Z. Liu, J. Zhang, and W. Liu (2014), AMOC response to global warming: dependence on the background climate and response timescale, *Clim. Dyn.*, *44*(11), 3449–3468, doi:10.1007/s00382-014-2165-x.

Zickfeld, K., et al. (2013), Long-term climate change commitment and reversibility: An EMIC intercomparison, *J. Clim.*, *26*(16), 5782–5809, doi:10.1175/JCLI-D-12-00584.1.